Tests of the hydrodynamic equivalence of direct-drive implosions with different D_2 and ^3He mixtures

J. R. Rygg, J. A. Frenje, C. K. Li, F. H. Séguin, and R. D. Petrasso[a)]
Plasma Science and Fusion Center, Massachusetts Institute of Technology, Cambridge, Massachusetts 02139

J. A. Delettrez, V. Yu Glebov, V. N. Goncharov, D. D. Meyerhofer,[b)] S. P. Regan, T. C. Sangster, and C. Stoeckl
Laboratory for Laser Energetics, University of Rochester, Rochester, New York 14623

(Received 17 February 2006; accepted 14 March 2006; published online 10 May 2006)

Direct drive implosions of targets filled with different mixtures of D_2 and ^3He gas on the OMEGA laser system [T. R. Boehly *et al.*, Opt. Commun. **133**, 495 (1997)] have shown an unexpected scaling of experimental nuclear yields. At temperatures above a few electron volts, D_2 and ^3He gases are fully ionized, and hydrodynamically equivalent fuels with different ratios of D_2 and ^3He can be chosen to have the same mass density, total particle density, and equation of state. Implosions with a 50/50 mixture of D:^3He by atom consistently result in measured nuclear yields half of that anticipated by scaling from measured yields of implosions with pure D_2 and nearly pure ^3He. This observation is seen over a wide range of experimental configurations, including targets with a variety of shell thicknesses and fill pressures, simultaneously for two different nuclear yields (DD and D^{3}He), and for shock and compression yields. A number of possible mechanisms to cause the scaling are considered, but no dominant mechanism has been identified. © *2006 American Institute of Physics*. [DOI: 10.1063/1.2192759]

I. INTRODUCTION

Ignition and high gain in inertial-confinement fusion[1–3] (ICF) requires an understanding of how the choice of materials affects implosion dynamics. ICF ignition targets are typically spherical capsules with an outer shell made of plastic or beryllium, a cryogenic layer of deuterium-tritium (DT) ice, and gaseous DT at the center. The direct-drive approach to ICF[4] implodes the target by direct illumination using multiple laser beams. Laser ablation of the outer surface of the capsule drives the remaining payload inward, compressing and heating it to a state where nuclear fusion can occur.

Surrogate materials or configurations provide a convenient test bed to study different aspects of ignition designs.[5,6] These surrogates are chosen to best mimic the implosion characteristics of the original design. For example, although ignition designs use an equal-mole DT mixture, pure D_2 is commonly used as a surrogate. However, the different mass densities can cause a difference in implosion dynamics (in particular through the Atwood number, which differs by a factor of 2 at the fuel-shell interface during the deceleration phase[7]).

To explore the effects of fill composition on implosion dynamics of surrogate fuels, a series of experiments using different ratios of D_2 and ^3He was performed. Evaluation of surrogate materials is best done when the materials are chosen to be as nearly hydrodynamically equivalent as possible. D and ^3He have the special property that they have the same value of $(1+Z)/A$, allowing mixtures of D_2 and ^3He to be chosen such that the mass density and the total particle density upon full ionization are identical. This results in the same Atwood number (affecting hydrodynamic instabilities[2,7]) and the same equation of state (EOS).

An additional advantage of these surrogate targets is that products from the DD nuclear reaction can be measured for all mixtures, whereas measuring the DD products from a DT implosion has proven difficult for ignition relevant implosions due to the large background of DT neutrons. A final advantage of D_2 and ^3He mixtures is their emission of D^{3}He protons that have been extensively used to diagnose ICF implosions at OMEGA.[8–10] Section II is a description of the setup and diagnostics used in the experiments. Section III describes the yield scaling expected of hydrodynamically equivalent implosions. Section IV describes the results observed in the experiments, as well as comparisons to the expected scaling and to one-dimensional (1-D) rad-hydro simulations. Section V discusses possible explanations, and a summary is given in Sec. VI.

II. EXPERIMENTAL SETUP

Direct-drive implosions were conducted at OMEGA,[11] with 60 beams of frequency-tripled (351 nm) UV light in a 1 ns square pulse and a total energy of 23 kJ. SG4 phase plates,[12] and two-dimensional (2-D), 1 THz bandwidth smoothing by spectral dispersion of the laser beam were used;[13] the beam-to-beam energy imbalance was typically between 2% and 4% rms. The spherical targets were plastic (CH) shelled capsules with diameters between 860 and 880 μm, wall thickness of 15, 20, 24, or 27 μm, and a flash coating of about 0.1 μm of aluminum.

[a)]Visiting Senior Scientist at LLE.
[b)]Also at Departments of Mechanical Engineering and Physics and Astronomy.

The gaseous fill of the capsules was composed of mixtures of D_2 and ^{3}He such that the atomic composition varied from pure D to nearly pure ^{3}He. Two classes of fill pressure were used—low (equivalent to 3 atm D_2) and high (equivalent to 15 atm D_2)—with predicted convergence ratios of 37 and 14, respectively. The mixtures within each class are considered hydrodynamically equivalent in that they have the same mass density (and therefore the same Atwood number during the deceleration phase), and, upon full ionization (above a few electron volts), the same total particle density, and EOS (ideal monatomic).

Capsule fills are hydrodynamically equivalent if the fill pressures of D_2 (X atm) and ^{3}He (W atm) are chosen to obey

$$X + \frac{3}{4}W = X_0, \tag{1}$$

where X_0 is the hydrodynamically equivalent pure D_2 fill pressure, in this paper equal to either 3 or 15 atm. The deuterium ion fraction by atom f_D scales with X and X_0 as

$$f_D = \frac{3X}{X + 2X_0}. \tag{2}$$

Since there are only two components to the fill gas, $f_{^3\mathrm{He}} = 1\text{-}f_D$.

Two standard gas mixtures were used to fill targets of all types: pure D_2 (f_D=1.0), and a D_2-^{3}He mixture with a 1:1 atomic ratio (f_D=0.5). A series of shots with different mixtures of D_2 and ^{3}He was undertaken for the 20 and 24 μm thick, high pressure capsules. In addition to the premixed, f_D=1.0 and 0.5 compositions, compositions with f_D=0.07, 0.27, and 0.78 were used.[14]

The error in the fill composition for the "standard" (f_D =0.5) D_2-^{3}He mixture is about 1% of f_D, since it comes premixed. Fill composition errors for the other composition ratios, which must be mixed to order, are also small: less than 3% of f_D.[15] This error estimate includes uncertainties in the original fill pressure, as well as uncertainties in the leak rates of D_2 and ^{3}He through the storage cell, and through the target shell as it is handled before shot time. The total fill pressure is known to better than 10%, and is independent of the fill composition.[15]

The following primary nuclear reactions occur in implosions of targets filled with mixtures of D_2 and ^{3}He:

$$\begin{aligned} &\mathrm{D} + \mathrm{D} \rightarrow {}^3\mathrm{He} + n(2.45\ \mathrm{MeV}), \\ &\mathrm{D} + \mathrm{D} \rightarrow \mathrm{T} + p(3.0\ \mathrm{MeV}), \\ &\mathrm{D} + {}^3\mathrm{He} \rightarrow {}^4\mathrm{He} + p(14.7\ \mathrm{MeV}), \end{aligned} \tag{3}$$

where the number in parentheses is the mean birth energy of the second product. Figure 1 shows the temperature dependence of the thermal reactivities of the D^{3}He reaction and the n-branch of the DD reaction, as determined by Bosch and Hale.[16] The branching probability of the n- and p-branches of the DD reaction are nearly equal over the temperatures of interest.

The principle diagnostics for this work were neutron time-of-flight (nTOF) scintillators[17] to measure the neutron

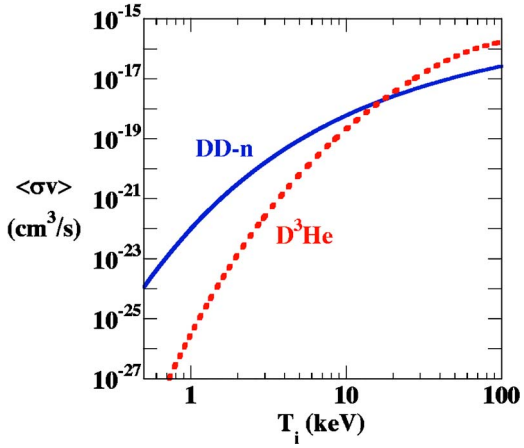

FIG. 1. (Color online) DD-n and D^{3}He thermal reactivities as a function of ion temperature.

branch of the DD reaction, and multiple wedge-range-filter (WRF) proton spectrometers[8] to measure the protons from the D^{3}He reaction. The nTOF detectors measure neutron yield and DD-burn averaged ion temperature, determined from the Doppler broadening of the neutron signal.

The WRF spectrometers measure the D^{3}He proton spectrum with high resolution (~100 keV). Transient magnetic fields[18] in the implosion corona can redistribute the initially isotropic proton flux emitted by the capsule by 20% rms (typical).[8] The average of multiple (2 to 7) spectrometers is used to obtain an estimate of the total yield. The mean downshift of the D^{3}He protons from their birth energy of 14.7 MeV is used to infer the areal density (ρR) of the imploded capsule averaged over the D^{3}He proton production.[8]

An alternative measurement of the burn-averaged ion temperature is given by the "ratio method."[19] The ratio of primary yields can be used to infer the ion temperature using the thermal reactivities (Fig. 1) and the fuel composition. The ratio of DD-n to D^{3}He reactivities changes by more than three decades from 1 to 10 keV, giving a determination of temperature that is not highly sensitive to the exact yields. Differences in burn duration or burn volume of the two constituent reactions result in only minor corrections to the inferred temperature (for example, see the very similar burn histories for DD-n and D^{3}He compression in Fig. 2). This correction is small, mainly because both reactions are dominated by the high-temperature region near the center.

Temporal diagnostics of the nuclear products include the neutron temporal diagnostic (NTD)[20] for measuring the DD-n burn history, and the proton temporal diagnostic (PTD) for measuring the D^{3}He burn history.[21,9] The D^{3}He burn history typically exhibits two periods of proton emission[22]—the first is the "shock burn," that occurs after the first convergence of the shock, near the end of the coasting phase, and before the capsule has fully compressed. About 300 ps later is the "compression burn" (see Fig. 2), which occurs during the deceleration and stagnation phases. Spectral measurements of the emitted D^{3}He protons from such capsules can often be decomposed into such "shock" and "compression" components, due to the different areal densities they pass through while escaping the capsule (~10 mg/cm^2 at shock

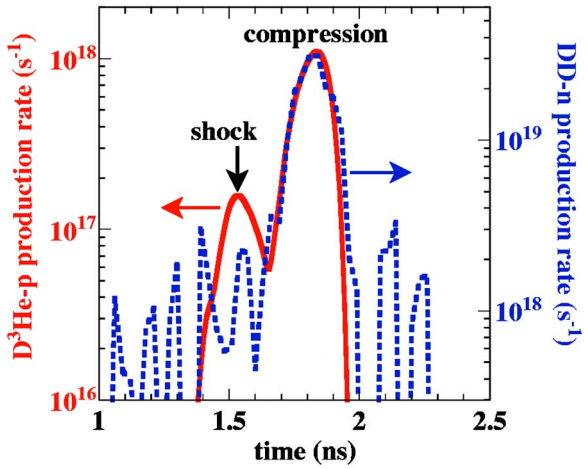

FIG. 2. (Color online) Measured D^3He proton (solid red) and DD-n (dashed blue) nuclear production histories of a 24 μm thick CH shell filled with 6 atm of D_2 and 12 atm of ^3He (shot 38525). Distinct shock and compression components are seen in the D^3He production history, whereas there is no evidence of neutrons at shock time in the DD-n production history. The noise level in the burn histories is about 10^{18}/s for DD-n, and less than 10^{16}/s for D^3He.

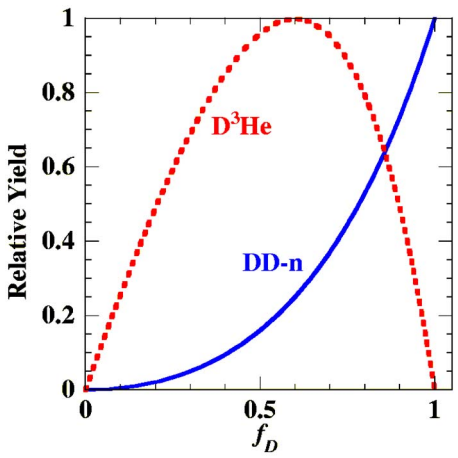

FIG. 3. (Color online) Yield dependence of the DD-n and D^3He reactions on the D fraction by atom (f_D).

and ~60 mg/cm^2 during compression). Due to the much weaker temperature dependence of the DD-n reactivity, the contribution of the high-temperature, low-density shock-burn phase to the total yield is much lower than for D^3He (typically 0.5%–1% rather than 5%–20%).

1-D rad-hydro simulations of these implosions were done using the code LILAC[23] with a flux limiter of 0.06. Composition scaling simulations were run by changing the initial fill composition, while using the same target and laser conditions. In order to obtain yields of both reactions using compositions of f_D=0.0 and 1.0, the results of those simulations were postprocessed as having a trace of the minority species.

III. EXPECTED SCALING

The nuclear yield is the spatial and temporal integral of the product of reactant densities times the temperature-dependent thermal reactivity of the nuclear reaction under consideration:

$$Y_n = \int \frac{1}{2} n_D^2(\vec{r},t)\langle\sigma v\rangle_{DD\text{-}n} d^3\vec{r}dt,$$
$$Y_p = \int n_D(\vec{r},t) n_{^3He}(\vec{r},t)\langle\sigma v\rangle_{D^3He} d^3\vec{r}dt, \quad (4)$$

where Y_n and Y_p are the DD neutron and D^3He proton yields, respectively, n_D and $n_{^3He}$ are the number densities of D and ^3He, respectively, and $\langle\sigma\nu\rangle$ is the local thermal reactivity averaged over a Maxwellian ion velocity distribution with temperature T_i. The particle densities and ion temperature will in general be functions of position and time. The factor of $1/2$ in the DD-n yield accounts for the double-counting of identical reactants.

For the hydrodynamically equivalent mixtures of D_2 and ^3He considered here, and using the relation $n_i=\rho/Am_p = \rho/(3-f_D)m_p$, the yields can be re-expressed in terms of f_D:

$$Y_n = \frac{f_D^2}{(3-f_D)^2}\int \frac{\rho^2(\vec{r},t)}{2m_p^2}\langle\sigma v\rangle_{DD\text{-}n} d^3\vec{r}dt,$$
$$Y_p = \frac{f_D(1-f_D)}{(3-f_D)^2}\int \frac{\rho^2(\vec{r},t)}{m_p^2}\langle\sigma v\rangle_{D^3He} d^3\vec{r}dt, \quad (5)$$

where m_p is the proton mass and ρ is the mass density. The factor $(3-f_D)^2$ is equal to A^2, and adjusts for the slightly different ion number densities of D_2 and ^3He plasmas at equal mass density. The advantage of this form is that the dependence on the fill composition, that determines the difference between hydro-equivalent targets, is taken out of the integral.

Figure 3 shows the predicted scaling of the DD neutron and D^3He proton yields as a function of fill composition for hydro-equivalent fuels. Although the character of the composition scaling is very different for the different nuclear reactions, both curves are independent of the implosion dynamics, so that the composition contribution to the yield can be factored out.

All subsequent yields in this paper will be scaled according to Eq. (6), unless otherwise noted:

$$\tilde{Y}_n = Y_n \frac{(3-f_D)^2}{f_D^2},$$
$$\tilde{Y}_p = Y_p \frac{(3-f_D)^2}{f_D(1-f_D)}, \quad (6)$$

where $\tilde{Y}_n$ and $\tilde{Y}_p$ denote the scaled DD-n and D^3He yields, respectively.

IV. EXPERIMENTAL OBSERVATIONS

The hydrodynamic equivalence of D_2 and ^3He mixtures is most clearly demonstrated by measurements of implosion timing. The time of peak neutron emission (DD-n bang time), as well as the duration of the neutron emission [characterized by the full width at half-maximum (FWHM) as measured by the NTD] are independent of f_D. In addition, the time of peak proton emission during the compression

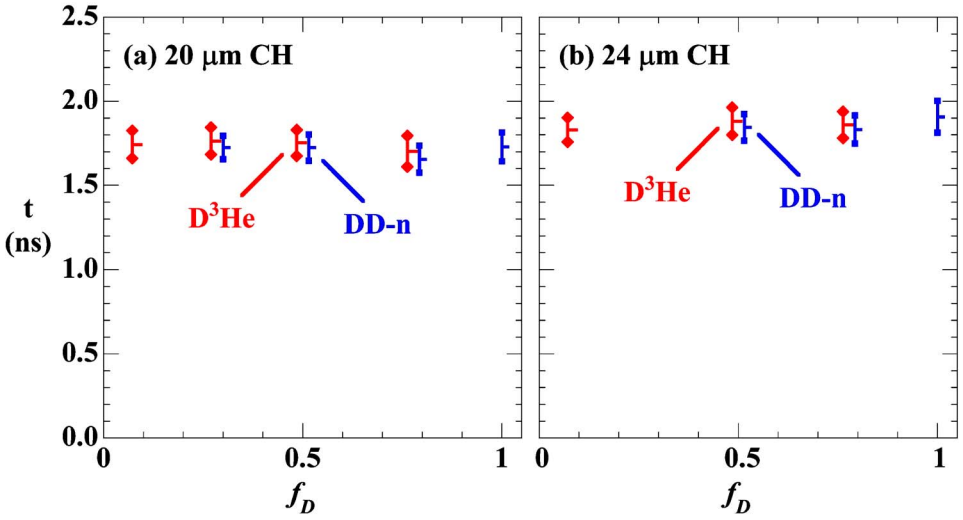

FIG. 4. (Color online) Nuclear bang time and burn duration as a function of fill composition, for implosions with (a) 20 μm and (b) 24 μm of CH. Red diamonds and blue squares are the times of half-maximum of peak emission of the D^3He protons and DD-neutrons, respectively.

phase (D^3He compression bang time), and the duration of proton emission (characterized by the FWHM of the compression peak as measured by PTD) are also independent of f_D. Figure 4 plots the bang time and burn duration of both nuclear products as a function of f_D for both 20 and 24 μm thick CH shells. Bang times and burn durations of the two nuclear products are also in good agreement with each other, an example of which can be seen fully in Fig. 2.

The measured yield of these hydrodynamically equivalent implosions deviates from the anticipated scaling shown in Fig. 3. The deviation of the scaled DD-n and D^3He compression yields ($\tilde{Y}_n$ and $\tilde{Y}_{p\text{-}c}$) for 20 and 24 μm CH shells with high pressure fills is shown in Fig. 5. The yields have been scaled to the fill composition according to Eq. (6), and in addition have been normalized to the yield at f_D=0.5, to

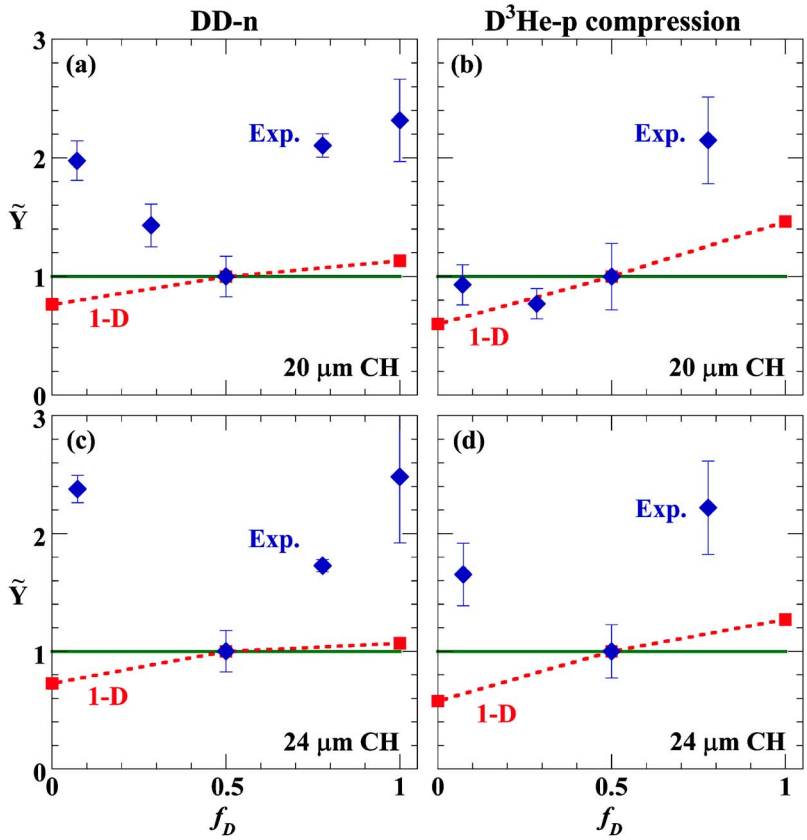

FIG. 5. (Color online) Scaled DD-n and D^3He compression yields for high pressure (X_0=15 atm) fills of shells with 20 and 24 μm of CH. (a) $\tilde{Y}_n$, 20 μm; (b) $\tilde{Y}_{p\text{-}c}$, 20 μm; (c) $\tilde{Y}_n$, 24 μm; (d) $\tilde{Y}_{p\text{-}c}$, 24 μm. All yields have been scaled to fill composition according to Eq (6), and normalized to the yields at f_D=0.5. True hydro-equivalent implosions would scale to the same yield (solid green line). 1-D simulations with LILAC (red squares, dotted) deviate slightly from hydro-equivalence, but not nearly as much as experimental measurements (blue diamonds). Diamonds are the average yield and standard deviation from similar capsules. The 20 μm plots show data reduced from a total of 42 shots, and the 24 μm plots show data reduced from a total of 24 shots.

TABLE I. Absolute (unscaled) compression yields of DD-n for $f_D=1.0$ and 0.5 shots, and D^3He for $f_D=0.5$ shots, as observed experimentally and as calculated by LILAC. The experimental yield over calculated yield (YOC) is also shown.

		$f_D=1.0$	$f_D=0.5$	
Shell	Type	Y_n ($\times 10^{10}$)	Y_n ($\times 10^{10}$)	$Y_{p\text{-}c}$ ($\times 10^{8}$)
	Observed	18.7	1.29	6.28
20 μm CH	Calculated	44.6	6.29	18.4
	YOC	42.0%	20.5%	34.1%
	Observed	9.0	0.58	1.46
24 μm CH	Calculated	18.7	2.80	4.22
	YOC	48.1%	20.7%	34.6%

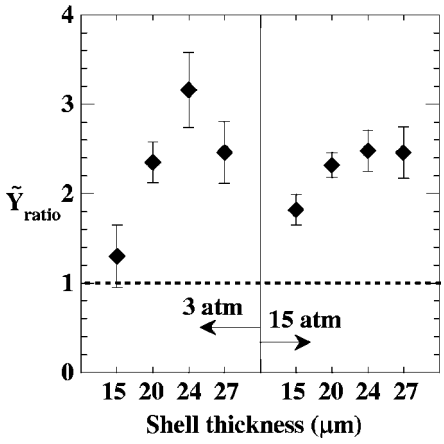

FIG. 6. The ratio of measured $\tilde{Y}_n$ for $f_D=1.0$ shots over $\tilde{Y}_n$ for $f_D=0.5$ shots. The ratio anticipated by the scaling in Fig. 3 is one (horizontal dotted line) for all target parameters. The points are the ratio of scaled average yields, and the errors are the quadrature sum of the standard deviations of the mean of the two fill compositions. The plot shows data reduced from 118 shots.

emphasize the composition scaling for different measurements. Yields from targets with D-rich and ^3He-rich fuels are typically twice as high as yields from targets with $f_D=0.5$. This trend is seen for both DD-n and D^3He yields, and for both 20 and 24 μm shells.[24]

This observed deviation is not seen in 1-D simulations (dashed line in Fig. 5), which instead more nearly follow the hydro-equivalent scaling, with only minor deviations. Table I shows the absolute yields of the normalization points at $f_D=0.5$, as observed experimentally and as calculated by LILAC, as well as the absolute DD-n yield at $f_D=1.0$. The DD-n experimental yield over calculated yield (YOC) is 21% for $f_D=0.5$, and 42% or 48% for $f_D=1.0$.

Comparison of the YOC for DD-n and D^3He on shots with $f_D=0.5$ illustrates the utility of simultaneous measurement of two nuclear reactions. As shown in Table I, the D^3He compression YOC is about 35%, compared to the DD-n YOC of 21%. The difference in the YOCs for the two nuclear reactions is due to their probing the deviation between the simulated and actual implosion in different ways as a result of their different temperature sensitivities.

The "factor of two" deviation of the yield scaling seen in these 20 and 24 μm CH shell, high pressure composition campaigns has also been seen over a diverse set of target configurations. Targets with 15, 20, 24, and 27 μm thick CH shells, and with both high and low fill pressure, were filled with the two standard compositions: $f_D=1.0$ and 0.5. Implosions of targets with both composition types emit DD-neutrons, and thus a comparison of $\tilde{Y}_n$ for like implosions with different compositions was done. Figure 6 shows the ratio of scaled yields, $\tilde{Y}_n\,[f_D=1.0]/\tilde{Y}_n\,[f_D=0.5]$ for these implosions. The points at 15 atm, and at 20 and 24 μm are the same as the points at $f_D=1.0$ in parts (a) and (c) of Fig. 5. Data reduced from 118 shots predominantly give a ratio greater than 2, where a ratio of 1 is anticipated for all capsule types.

The observed ion temperatures are not sufficient to explain the observed yield deviation. The mean ion temperature was measured using two methods: nTOF Doppler broadening and the yield ratio method. The nTOF does not show a trend in the ion temperature, whereas ion temperature from the ratio method suggests increasing temperatures for higher D content fuels (see Fig. 7). Postprocessing of 1-D LILAC simulations give burn-averaged temperatures that are not strongly dependent on fill composition. Areal density measurements using the downshift of primary D^3He protons (D^3He fuels) or secondary D^3He protons (pure D_2 fuel) show a lower value at compression time for $f_D=0.5$ (for 24 μm shells) (Fig. 8), suggesting slightly less compression for those shots.

A similar deviation from the anticipated scaling is also seen for the D^3He shock yield ($\tilde{Y}_{p\text{-}s}$), which is emitted about 300 ps earlier than the compression yield, and is produced under very different conditions, before the start of the deceleration phase and the onset of turbulent mixing,[22] at temperatures twice as high as that at compression time, and at mass densities less than 10% those at compression time. Figure 9 shows the scaled D^3He shock yield and the shock-yield-averaged ρR for implosions with 24 μm CH shells. The results at shock time are reminiscent of the results at compression time, with lower scaled yield and ρR for the $f_D=0.5$ shots than for D-rich or ^3He-rich mixtures.

A summary of results from figures in this section is listed in Table II for different mixtures of high pressure fills in shells with 20 and 24 μm of CH.

V. DISCUSSION

A closer look at the possibility of a measurement error is certainly warranted when observations deviate so far from the scaling derived from simple principles, as well as from computer simulations. The individual measurement error on a given shot is about 10% for both DD-n and D^3He yields; however, the shot-to-shot yield variation for nominally identical shots is closer to 20% rms. Averaging the results from many like shots reduces the standard deviation of the mean considerably, in most cases below 10%. Systematic yield uncertainties in the diagnostics are unlikely to cause the yield

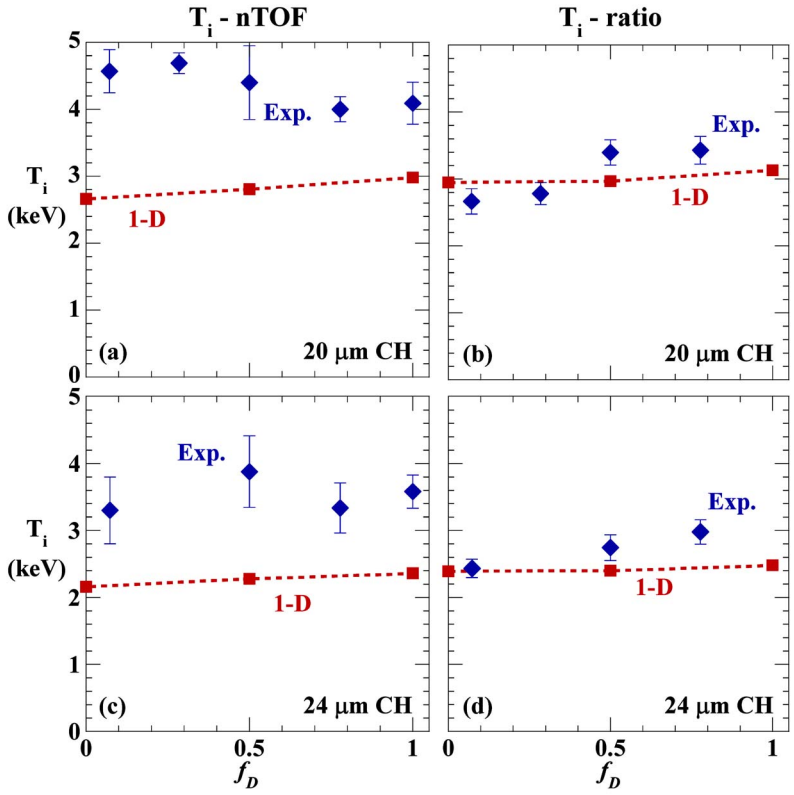

FIG. 7. (Color online) Ion temperature as a function of fill composition, as determined by nTOF for high pressure fills of (a) 20 μm and (c) 24 μm shells, and using the ratio method for (b) 20 μm and (d) 24 μm. Diamonds: average and standard deviation of experimental observations. Squares and dotted line: 1-D LILAC.

scaling. The yield measurements for the two nuclear reactions use different diagnostics, using different principles, yet measured the same deviation.

From Eq. (4), the deviation in the yield scaling must then be explained through differences in composition, temperature, density, burn volume, or burn duration of the target during the implosion. According to temporal measurements of nuclear burn histories, the implosion timing does not depend on the fill composition. Uncertainty in the composition is at most a couple of percent, which is not enough to affect the yields by a factor of 2. In addition, composition errors affect the DD-n and D^3He yield scaling in different ways (Fig. 3), yet the same deviation is seen for both.

The observed trend of the ratio-inferred ion temperature could be part of the story, due to the strong dependence of the thermal reactivities of both reactions at the temperatures of interest. The DD-n and D^3He reactivities scale approximately as T_i^4 and T_i^7, respectively, near T_i=3 keV. A linear fit through the observed ratio-inferred T_i in Fig. 7(d) was used

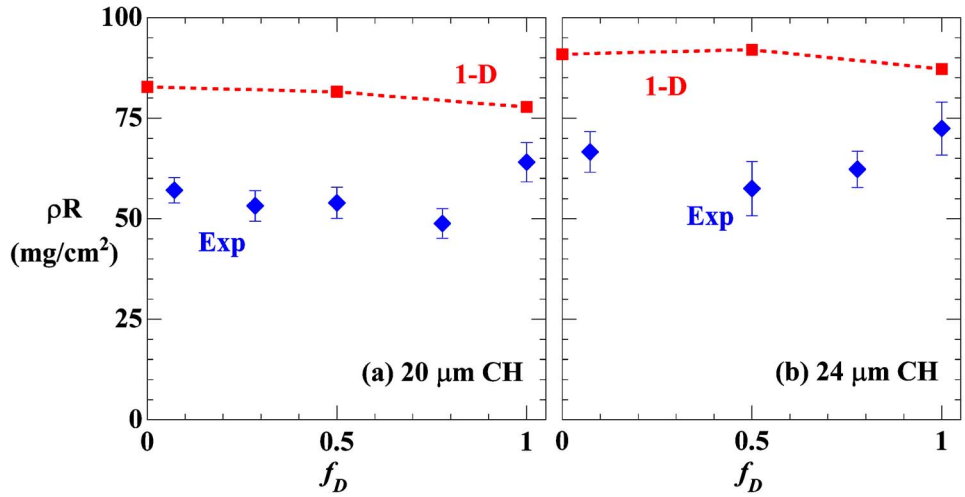

FIG. 8. (Color online) Inferred compression-burn-averaged ρR as a function of fill composition, for high pressure fills of 20 μm (a) and 24 μm (b) thick shells. Diamonds: average and standard deviation of experimental observations. Squares and dotted line: 1-D LILAC. For each plot, higher ρR. corresponds to more compression, since all targets started with the same shell thickness.

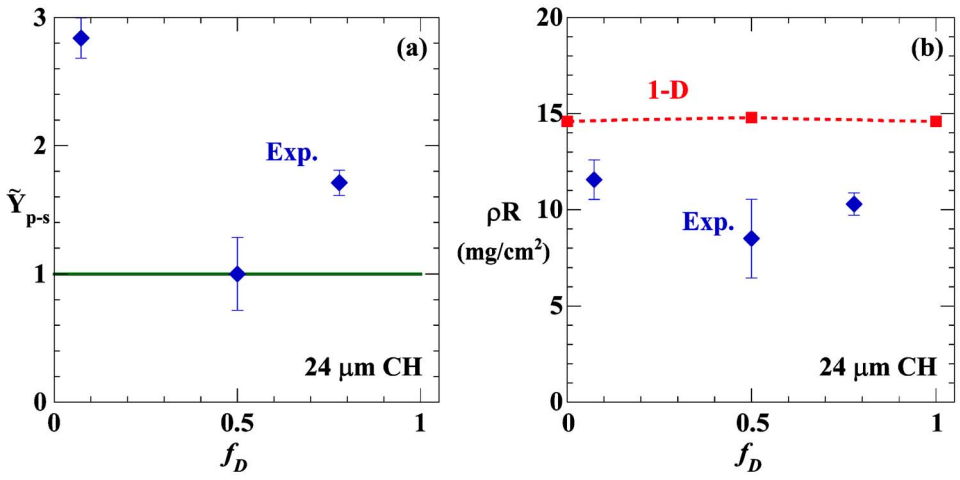

FIG. 9. (Color online) D^3He shock results for 24 μm CH capsules. (a) Scaled shock yield and (b) shock-yield-averaged ρR as a function of fill composition. Solid line: hydro-equivalent scaling. Squares and dotted line: 1-D LILAC. Diamonds: average and standard error of experimental observations.

to adjust the hydro-equivalent $\tilde{Y}_n$ scaling. The solid curve in Fig. 10(a) plots this T_i-ratio yield scaling against the observed yields from Fig. 5(c). This corrected scaling looks better for D-rich fuels, but deviates further than the uncorrected hydro-equivalent scaling from the observed yields for ^{3}He-rich fuels. Since there was no clear trend in the nTOF-derived temperatures, a similar yield scaling fit was not done using the nTOF temperatures.

The two remaining factors of fuel density and burn volume are related to the compression of the capsule, which can be inferred by measurements of ρR. A simple model of the implosion, which assumes that the shell temperature and shell aspect ratio at bang time does not depend on fill composition, determines that the yield scales approximately as $(\rho R)^3$. The open circles in Fig. 10(b) plots this ρR yield scaling against the observed yields from Fig. 5(c). Higher ρRs were observed for high and low D concentrations compared to the 50/50 mixture. The shape predicted from the $(\rho R)^3$ scaling is in qualitative agreement with the measurements, though it does not show quite as strong a scaling.

Although additional measurements suggest that some combination of ion temperature and density might be sufficient to explain the observed yield deviation, these factors must come from some physical mechanism, a number of which will be explored below.

The deviation from the assumed hydro-equivalence is unlikely to be explained by 2-D or 3-D hydro effects, including hydrodynamic instabilities and turbulent mixing that would reduce the burn volume and truncate the burn duration. A similar trend was experimentally observed over a wide range of physical situations in which 2-D hydro effects would likely have behaved very differently. Implosions with thicker shells are considered to be more hydrodynamically stable,[25] yet the same yield trend is seen for 20 and 24 μm shells with high fill pressure. Implosions with low fill pressure are considered less hydrodynamically stable, yet the yield trend is the same as for high fill pressure (Fig. 6). A similar trend is also seen for D^3He shock-burn measurements, despite the fact that it has been shown that there is no atomic level mixing in the burn region at shock time.[22] Thus, pure hydrodynamics can not explain the observed differences.

A wealth of data seems to exclude pure hydrodynamic differences between these mixtures as the mechanism for the

TABLE II. D fraction by atom, number of shots averaged, DD-n, D^3He compression, and shock yields (scaled by fill composition and normalized to $f_D=0.5$), ion temperature, areal density, and DD bang time for high pressure fills of two different shell thicknesses.

Shell	f_D	Number of shots	$\lvert\tilde{Y}_n\rvert$	$\lvert\tilde{Y}_{p\text{-}c}\rvert$	$\lvert\tilde{Y}_{p\text{-}s}\rvert$	T_i-nTOF (keV)	T_i ratio (keV)	ρR (mg/cm^2)	t_{bang} (ns)
CH 20 μm	1.00	22	2.32	—	—	4.1	—	64	1.73
	0.78	5	2.10	2.15	0.77	4.0	3.4	49	1.65
	0.50	8	1.00	1.00	1.00	4.4	3.4	54	1.72
	0.28	4	1.43	0.77	0.85	4.7	2.8	53	1.73
	0.07	3	1.98	0.93	1.23	4.6	2.7	57	—
CH 24 μm	1.00	10	2.48	—	—	3.6	—	72	1.91
	0.78	2	1.73	2.22	1.71	3.3	3.0	62	1.83
	0.50	9	1.00	1.00	1.00	3.9	2.7	58	1.87
	0.07	3	2.38	1.65	2.84	3.3	2.4	67	—

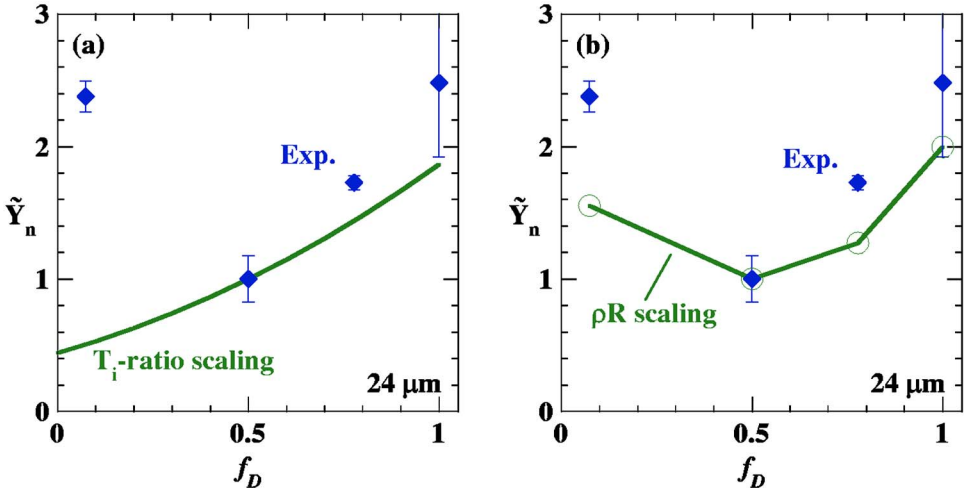

FIG. 10. (Color online) Measured (blue diamonds) DD-n yields as a function of f_D for 24 μm shells with high pressure, from Fig. 5(c). In these plots, the hydro-equivalent scaling has been adjusted to take into account effects of measured ion temperature and areal density on the yield. (a) The solid line is a T_i-corrected scaling curve, based on a linear fit to the experimental T_i ratios in Fig. 7(d). (b) The open circles and connecting line include a ρR correction based on the measured ρR values shown in Fig. 8(b).

observed variation in their yields (as it should be since they were chosen to be hydro-equivalent). The deviation from hydrodynamic equivalence is likely to be due to the microscopic details of the mixture. It may have something to do with the variation in the average Z in the fuel, which varies from 1 (pure D_2), to nearly 2 (^{3}He rich), the difference in ion masses, or a subtlety in the statistical treatment of mixtures.

Bremsstrahlung radiation scales as $\sim\rho^2 T_e^{1/2} Z^3/A^2$, which for these mixtures differs by a factor of 3.6 from pure D_2 (low) to pure ^{3}He, assuming the same density and temperature. A factor of 3 difference in the radiated power may then trigger differences in the absorption in the CH, and initiate changes in the implosion dynamics. However, the yield discrepancy trend is about the same for cases with significantly different radiative properties, such as for low pressure and high pressure fills, as well as at both shock and compression time. The difference in density in these scenarios radically affects the efficiency of bremsstrahlung radiation. In addition, the yield deviation is not monotonic with the D fraction, so that bremsstrahlung radiation seems unlikely as the sole mechanism.

Thermal conduction in these dynamic implosions can be difficult to calculate due to nonequilibrium conditions and other non-local effects. However, to get a sense of the scaling, consider Spitzer-Harm electron thermal conduction:[26]

$$q_{\mathrm{SH}} = -K\nabla T,$$

$$K \propto \delta(Z)\frac{T_e^{5/2}}{Zm_e^{1/2}\ln\Lambda}, \tag{7}$$

$$\delta(z) = \frac{Z+0.24}{Z+4.2}.$$

Ignoring the coulomb logarithm variation, pure D_2 has a 32% higher classical conductivity than pure ^{3}He, and 17% higher than the standard D_2-^{3}He mixture (using "average" ions). Ion thermal conduction has a similar form, but with a stronger Z dependence.[27] Ion conduction is relatively small when the ion and electron temperatures are equal, but can become important when the ion temperature is higher, such as for shock heating. However, for both types of thermal conduction, the trend is again monotonic with D fraction.

Shock heating initially puts most energy into heating the ions, with more energy going to heavier ions.[28] Equal-density mixtures of D_2 and ^{3}He will absorb the same total amount of energy from a shock front, but mixtures with a higher concentration of ^{3}He will have a higher initial ion temperature due to the higher average ion mass (and corresponding lower ion density). A slight difference in this initial state of the gas might, after compression, be enough to change the dynamics and the resulting nuclear yields. However, the compression condition will be quite a bit different for the different implosions types (high, low pressure; thin, thick shells), yet the same deviation is seen in many cases. It is also difficult to explain the nonmonotonic trend with this picture.

It is possible that there is stratification of the ion species during the deceleration phase. The scaled performance of the "pure" fuels seems to be greatest, so perhaps the mixture of different species is important. During the deceleration phase, the ^{3}He concentration might be slightly enhanced near the center. The hot center will then have a lower nuclear yield due to scarcer D ions. In this picture, though, the ^{3}He rich fuels should also have a reduced yield, so that the nonmonotonic trend is again a problem.

The plausibility of stratification can be considered using simple arguments. Because of the high density during the compression phase, any concentration enhancement will have to come through a difference in diffusion of the D and ^{3}He ions. With plasma parameters typical of the fill early in the compression burn (4 keV, 3 g/cc), it is found that the time it takes even one particle to diffuse across the capsule is very much longer than the implosion time.

Kinetic effects could play an important role in the observed yield scaling. A non-Maxwellian velocity distribution could significantly alter nuclear production, particularly at the time of shock collapse, where the distribution is far from Maxwellian. It has also been suggested that yield degradation could result from the loss of ions in the tail of the distribution, which normally dominate the nuclear production.

The longer mean free paths of the ions in the tail may allow them to escape the fuel region if the $\rho R < 10$ mg/cm^2.[29] It is not sufficient, though, that kinetic effects only change the nuclear production; a kinetic effect must change the nuclear production nonmonotonically with D fraction, and by a factor of two between pure and mixed D and ^{3}He. Many processes to explain the observed yield scaling have been considered here, but no single mechanism is sufficient to explain the trend.

VI. SUMMARY

In summary, experimental observations of the scaling of nuclear yields from implosions with hydro-equivalent mixtures of D_2 and ^{3}He deviate from the scaling determined using a simple consideration of composition ratios, as well as from a scaling based on 1-D rad-hydro simulations. This deviation is particularly puzzling since the trend is not monotonic with D fraction—the scaled D^{3}He yield is lower than the scaled yields on both the D_2-rich and ^{3}He-rich sides.

The same scaling deviation is observed in diverse physical situations, including implosions of targets with initial fill pressures of 3 and 15 atm, and target shell thicknesses of 15, 20, 24, and 27 μm of CH. A similar yield scaling deviation is observed for both DD-n and D^{3}He yields, despite drastically different dependence of their yields on composition and temperature. Overall, a similar scaling deviation is seen for both the shock and compression components of the D^{3}He yield, corresponding to times separated by several hundred picoseconds, and reflecting very different plasma conditions.

It has been shown that measurements of the burn-averaged ion temperature, using two different methods, are insufficient to explain the entire yield scaling deviation. Errors in the initial fill composition of the D_2 and ^{3}He mixtures, and differences in the implosion timing have also been excluded. Measurements of the burn-averaged areal density, ρR, are suggestive that D_2 and ^{3}He mixtures with f_D near 0.5 might experience less compression, resulting in a lower yield.

A number of possible mechanisms to cause the scaling are considered, but no dominant mechanism has been identified. Differences in the radiative and transport properties of different D_2 and ^{3}He mixtures are included in 1-D simulations, but do not apparently have as great an effect on the yield as what was observed. Hydrodynamic instabilities in 2-D and 3-D appear to be ruled out. The initial gas state set by the converging shock, ion species stratification, and kinetic effects were also considered.

This study raises some concern as to the near equivalence of D_2 as a DT fuel surrogate for studying implosion dynamics. Even when the mass density of the D_2 and ^{3}He mixtures is the same, we see discrepancies in the yield, although it is not clear what mechanism causes the discrepancy, and whether it is due to a difference in average Z, in ion masses, or in transport properties of mixed materials. To explore such issues, further scrutiny of the ion conductivity and its effects on implosion dynamics is underway by one of us (Goncharov), which may be an important factor due to its strong Z dependence.

Investigation of the yield scaling at constant Z could be accomplished by using different fuel mixtures, including mixtures of D and T, and an extension of this study with mixtures of D_2, ^{3}He, and either H_2 or ^{4}He. Experiments are being actively planned that would vary the D and T mixture with the aim of measuring simultaneously the absolute yield of both DT and DD,[30] the results of which will have direct relevance for the fills of ignition targets, and will take us a step closer to understanding the present conundrum.

ACKNOWLEDGMENTS

The authors express their gratitude to the OMEGA engineers and operations crew who supported these experiments. This work was supported in part by the U.S. Department of Energy Office of Inertial Confinement Fusion (Grant No. DE-FG03-03NA00058), by the Lawrence Livermore National Laboratory (Subcontract No. B543881), and by the Laboratory for Laser Energetics (Subcontract No. 412160-001G) under Cooperative Agreement DE-FC52-92SF19460, University of Rochester, and New York State Energy Research and Development Authority.

[1] J. Nuckolls, L. Wood, A. Theissen, and G. Zimmerman, Nature (London) **239**, 139 (1972).
[2] J. D. Lindl, *Inertial Confinement Fusion* (Springer, New York, 1999).
[3] S. Atzeni and J. Meyer-ter-Vehn, *The Physics of Inertial Fusion* (Oxford University Press, New York, 2004).
[4] S. E. Bodner, D. G. Colombant, J. H. Gardner *et al.*, Phys. Plasmas **5**, 1901 (1998).
[5] F. J. Marshall, J. A. Delettrez, V. Yu. Glebov *et al.*, Phys. Plasmas **7**, 1006 (2000).
[6] R. L. McCrory, R. E. Bahr, R. Betti *et al.*, Nucl. Fusion **41**, 1413 (2001).
[7] S. P. Regan, J. A. Delettrez, V. Yu. Glebov *et al.*, Bull. Am. Phys. Soc. **47**, 113 (2005).
[8] F. H. Séguin, J. A. Frenje, C. K. Li *et al.*, Rev. Sci. Instrum. **74**, 975 (2003).
[9] J. A. Frenje, C. K. Li, F. H. Séguin *et al.*, Phys. Plasmas **11**, 2798 (2004).
[10] F. H. Séguin, J. L. DeCiantis, J. A. Frenje *et al.*, Rev. Sci. Instrum. **75**, 3520 (2004).
[11] T. R. Boehly, D. L. Brown, R. S. Craxton *et al.*, Opt. Commun. **133**, 495 (1997).
[12] F. J. Marshall, J. A. Delettrez, R. Epstein *et al.*, Phys. Plasmas **11**, 251 (2004).
[13] S. Skupsky and S. Craxton, Phys. Plasmas **6**, 2157 (1999).
[14] The $f_D = 0.78$ shots plotted on the 20 μm CH subfigures actually had 19 μm thick shells.
[15] M. Bonino (private communication).
[16] H.-S. Bosch and G. M. Hale, Nucl. Fusion **32**, 611 (1992).
[17] R. A. Lerche and T. J. Murphy, Rev. Sci. Instrum. **63**, 4880 (1992).
[18] Tangential electric fields have not been excluded as the cause for the anisotropic proton emission, but for these implosions there is no radial E field when the protons are emitted.
[19] C. K. Li, D. G. Hicks, F. H. Séguin *et al.*, Phys. Plasmas **7**, 2578 (2000).
[20] R. A. Lerche, D. W. Phillion, and G. L. Tietbohl, Rev. Sci. Instrum. **66**, 933 (1995).
[21] C. Stoeckl, V. Yu. Glebov, S. Roberts *et al.*, Rev. Sci. Instrum. **74**, 3 (2003).
[22] R. D. Petrasso, J. A. Frenje, C. K. Li *et al.*, Phys. Rev. Lett. **90**, 095002 (2003).
[23] J. Delettrez, R. Epstein, M. C. Richardson *et al.*, Phys. Rev. A **36**, 3926 (1987).
[24] Except for the D^{3}He yield from ^{3}He-rich, 20 μm thick target implosions.
[25] S. P. Regan, J. A. Delettrez, V. N. Goncharov *et al.*, Phys. Rev. Lett. **92**, 185002 (2004).
[26] L. Spitzer and R. Harm, Phys. Rev. **89**, 977 (1953).
[27] S. I. Braginskii, Plasma Phys. **1**, 205 (1965).
[28] Ya. B. Zel'dovich and Yu. P. Raizer, *Physics of Shock Waves and High-*

Temperature Hydrodynamic Phenomena, edited by W. D. Hayes and R. F. Probstein. (Dover Mineola, NY 2002).
[29]D. Henderson, Phys. Rev. Lett. **33**, 1142 (1974).
[30]Only recent technological advances have made the detection of DD neutrons in the background of DT neutrons feasible. See V. Yu Glebov, "Development of Nuclear Diagnostics for the National Ignition Facility," 16th Conference on High-Temperature Plasma Diagnostics (May 2006), to be published in Rev. Sci. Instrum.